PHYSICAL REVIEW FLUIDS **2**, 021901(R) (2017)

Data-driven approach to design of passive flow control strategies

F. Gómez* and H. M. Blackburn

Department of Mechanical and Aerospace Engineering, Monash University, Clayton, Victoria 3800, Australia

(Received 12 September 2016; published 7 February 2017)

An approach to designing passive devices for control of unsteady flows is presented. The method requires only snapshots of the flow to be controlled as inputs. A temporal correlation based on proper orthogonal decomposition of both fluctuating velocity and nonlinear forcing serves to identify the spatial locations in which the forcing drives the different unsteady flow features. The installation of a passive device in these spatial locations inhibits the fluctuating motion. The potential of the methodology is demonstrated via the suppression of vortex shedding in flow past a square cylinder, paving the way to the control of more complex flows using passive devices. Connections in agreement with previous studies targeting the same flow using different passive flow control strategies are provided.

DOI: 10.1103/PhysRevFluids.2.021901

Control of flow past bluff bodies is of importance owing to potential benefits in suppressing structural vibrations, mitigating acoustic noise, or reducing mean drag [1]. A large body of literature [1–5] has dealt with the effective use of passive devices in the wake past a bluff body to stabilize the fluctuating motion. The success of the passive devices, such as control cylinders or splitter plates, relies on their simplicity and lack of power input, however the design of such devices often requires a *trial and error* parameter sweep of different sizes, shapes, and locations owing to a lack of understanding of the flow control mechanisms [1].

While the concept of structural sensitivity introduced by Giannetti and Luchini [6] provides some physical insight into these mechanisms and allows design criteria for the use of passive devices, obtaining the structural sensitivity is a linear analysis, and special treatment, modeling, and care is required when dealing with unsteady or turbulent flows, far from a steady state. The structural sensitivity can be understood as the required changes in a steady flow in order to prevent the development of an unstable linear instability.

Here we introduce a generic methodology to design flow control strategies for unsteady flows using passive devices. The main differences with respect to the concept of structural sensitivity are that first, it directly deals with unsteady flows without assumptions and, second, the approach is data driven, hence it does not require the knowledge of a steady state or mean flow; only snapshots of the flow to be controlled are required to design a passive flow control strategy.

The theoretical framework underlying the present methodology is that of self-sustained flows inspected via the resolvent analysis of McKeon and Sharma [7], in which nonlinear forcing drives fluctuating velocities, which in turn generates nonlinear forcing. We focus on unsteady flows governed by the incompressible Navier-Stokes equations in nondimensional form

$$\nabla \cdot \hat{\boldsymbol{u}} = 0, \tag{1}$$

$$\partial_t \hat{\boldsymbol{u}} + \hat{\boldsymbol{u}} \cdot \nabla \hat{\boldsymbol{u}} = -\nabla p + \mathrm{Re}^{-1} \nabla^2 \hat{\boldsymbol{u}}, \tag{2}$$

where Re is the Reynolds number based on reference velocity U and length scale D, $\hat{\boldsymbol{u}} = (u, v, w)$ is the velocity vector expressed in Cartesian coordinates (x, y, z), and p is the modified pressure. A Reynolds decomposition can be applied to the total velocity $\hat{\boldsymbol{u}}$ to yield a fluctuating velocity $\boldsymbol{u} = \hat{\boldsymbol{u}} - \boldsymbol{u}_0$ by subtracting the temporal and spatial mean flow $\boldsymbol{u}_0$. The introduction of this

*francisco.gomez-carrasco@monash.edu

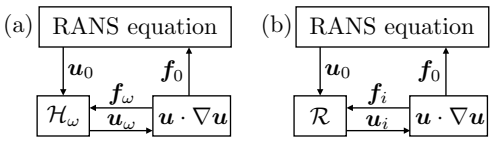

FIG. 1. Interpretation of the self-sustained flow framework. (a) Spectral formulation: The fluctuating nonlinear forcing $\boldsymbol{f}_\omega$ acts as the forcing that drives fluctuating velocities $\boldsymbol{u}_\omega$, which in turn generates nonlinear forcing. The time-average component of the nonlinear forcing, the Reynolds stress $\boldsymbol{f}_0$, modifies the mean flow $\boldsymbol{u}_0$ via the RANS equation. The feedback loop is completed with the mean flow characterizing the properties of the resolvent operator $\mathcal{H}_\omega$, i.e., how nonlinear forcing fluctuating drives the fluctuating velocity. (b) Discrete time-domain formulation, using velocity POD modes $\boldsymbol{u}_i$ and their correlated POD forcing $\boldsymbol{f}_i$. The operator $\mathcal{R}$ establishes a linear relation between the two set of fluctuating POD modes.

decomposition in Eq. (2) and a time averaging lead to the Reynolds-averaged Navier-Stokes (RANS) equation

$$\partial_t \boldsymbol{u}_0 + \boldsymbol{u}_0 \cdot \boldsymbol{\nabla} \boldsymbol{u}_0 = -\boldsymbol{\nabla} p + \mathrm{Re}^{-1} \nabla^2 \boldsymbol{u}_0 + \boldsymbol{f}_0, \tag{3}$$

with $\boldsymbol{f}_0$ denoting the Reynolds stress. This represents the contribution to the mean flow of the nonlinear interaction of the fluctuating velocity $\hat{\boldsymbol{f}} = \boldsymbol{u} \cdot \boldsymbol{\nabla} \boldsymbol{u}$. In a similar manner, the following relationship for the fluctuating velocity is obtained:

$$\partial_t \boldsymbol{u}(t) = \mathcal{L} \boldsymbol{u}(t) + \boldsymbol{f}(t), \tag{4}$$

where $\mathcal{L}$ is the Jacobian of the NSE and $\boldsymbol{f}$ is the fluctuating nonlinear forcing. Equation (4) can be Fourier filtered to any frequency ω to obtain

$$\boldsymbol{u}_\omega = \mathcal{H}_\omega \boldsymbol{f}_\omega, \tag{5}$$

in which $\mathcal{H}_\omega = (-i\omega \boldsymbol{I} - \mathcal{L})^{-1}$ is defined as the resolvent operator, with $\boldsymbol{u}_\omega$ and $\boldsymbol{f}_\omega$ being the Fourier-filtered fluctuating velocity and nonlinear forcing components at ω, respectively. The key result of (5) is that it shows that the linear relationship between fluctuating velocity and fluctuating nonlinear forcing is driven by the properties of the resolvent operator.

The combination of the RANS equation (3) with the resolvent relationship (5) leads to the classical picture of self-sustained flows sketched in Fig. 1(a). The fluctuating nonlinear forcing $\boldsymbol{f}_\omega$ acts as the forcing that drives fluctuating velocities $\boldsymbol{u}_\omega$, which in turn generates nonlinear forcing. The time-average component of the nonlinear forcing, the Reynolds stress $\boldsymbol{f}_0$, modifies the mean flow $\boldsymbol{u}_0$ via the RANS equation. The feedback loop is completed with the mean flow characterizing the properties of the resolvent operator $\mathcal{H}_\omega$, i.e., how nonlinear forcing drives the fluctuating velocity.

The outline above highlights the role of the resolvent operator in the self-sustained flow mechanisms. As such, a large number of recent papers have focused on the inspection of the properties of this operator in different flow configuration, such as pipes [7], channels [8], lid-driven cavities [9], cylinders [10], or backward-facing steps [11]. The key result in these investigations is that, under the presence of a dominant physical mechanism, the resolvent behaves like a selective directional amplifier. Consequently, a low-rank approximation of the operator can be exploited in order to extract physical features or generate reduced-order models. On the other hand, the ability to inspect of the resolvent operator is often limited due to its high dimensionality and limited availability of computational resources, especially in the case of three-dimensional flows. While the assembly and storage of the resolvent operator can lead to large computational memory requirements, its alternative strategy, the study of the action of the operator via time stepping, can also lead to large computational time requirements.

We propose an alternative data-driven strategy to circumvent the need to obtain the resolvent operator while still making use of this self-sustained flow framework. The data-driven approach is motivated by the empirical formulation in Fourier space proposed by Towne *et al.* [12], however

the present approach differs from the empirical resolvent decomposition in that we do not attempt a data-driven approach to inspect the resolvent operator. Although the obvious choice of data representation for this framework would be their Fourier transform, a number of difficulties arise when dealing with flow data in the form of snapshots. For instance, a Fourier transform of full data can be expensive to compute and relevant flow features may be composed of several frequencies, leading to several operations around the resolvent operator at different frequencies. For this reason, a more general framework is introduced in order to deal with snapshot data in a more efficient way, while maintaining the self-sustained framework. The temporal derivative ∂_t is linear, hence it is possible to write down a relationship between fluctuating velocity and nonlinear forcing in the form of

$$\boldsymbol{u}(t) = \mathcal{R}\boldsymbol{f}(t), \tag{6}$$

where $\mathcal{R} = (\partial_t - \mathcal{L})^{-1}$ can be understood as an impulse response function. Note that the particular case of a periodic fluctuating velocity with frequency ω leads to $\partial_t = -i\omega\mathcal{I}$ and the same resolvent operator in Eq. (5) could be obtained. The operator $\mathcal{R}$ is unknown in principle, because it depends on how the velocity changes in time, however the relationship (6) is the key to the investigation of flow dynamics from a data-driven point of view. We assume a set of s snapshots of the fluctuating velocity

$$\mathcal{U}(t) = [\boldsymbol{u}(t_1)\,\boldsymbol{u}(t_2)\,\cdots\,\boldsymbol{u}(t_s)] \tag{7}$$

and their corresponding fluctuating nonlinear terms, computed from $\hat{\boldsymbol{f}} = \boldsymbol{u}\cdot\nabla\boldsymbol{u}$,

$$\mathcal{F}(t) = [\boldsymbol{f}(t_1)\,\boldsymbol{f}(t_2)\,\cdots\,\boldsymbol{f}(t_s)]. \tag{8}$$

A low-rank proper orthogonal decomposition (POD) obtained via singular value decomposition (SVD) of the snapshot matrix $\mathcal{U}$ leads to

$$\mathcal{U}(t) = \sum_{i=1}^{r} \psi_i^u(\boldsymbol{x})\sigma_i^u\phi_i^u(t), \tag{9}$$

where $\psi_i^u(\boldsymbol{x})$ are the spatial POD modes, $(\sigma_i^u)^2$ represents the average kinetic energy of the ith POD mode, and $\phi_i^u(t)$ is the corresponding temporal evolution. Criteria for the selection of the rank $r \leqslant s$ are provided in what follows. The kinetic energy defined as the L_2 norm

$$\|\boldsymbol{u}\|^2 = \int_\Omega \boldsymbol{u}^T\cdot\boldsymbol{u}\,d\Omega = \boldsymbol{u}^T\mathcal{M}\boldsymbol{u} \tag{10}$$

is employed to perform POD, hence, in practice, a SVD is applied to the modified snapshot matrix $\hat{\mathcal{U}} = \sqrt{\mathcal{M}}\mathcal{U}T^{-1/2}$, where T is an identity matrix multiplied by the time span $t_s - t_1$. Note that, for simplicity, we have not distinguished between continuous or discretized operators. This scaling guarantees that the POD modes $\psi_i^u(\boldsymbol{x}) = \sqrt{\mathcal{M}^{-1}}\hat{\psi}_i^u(\boldsymbol{x})$ yield unit energy under the L_2 norm and that they are orthogonal to each other. Another key property is that the POD modes are also orthogonal in time,

$$(t_s - t_1)^{-1}\int_{t_1}^{t_s} \phi_i^{u*}(t)\phi_j^u(t)dt = \begin{cases} 1, & i = j \\ 0, & i \neq j, \end{cases} \tag{11}$$

hence it is trivial to show that the singular value $(\sigma_i^u)^2$ corresponds to the average kinetic energy of each POD mode. A POD can also be applied to the fluctuating forcing to obtain

$$\mathcal{F}(t) = \sum_{i=1}^{r} \psi_i^f(\boldsymbol{x})\sigma_i^f\phi_i^f(t), \tag{12}$$

in which the decomposition has been truncated to the same rank r as the POD velocity for simplicity. The two POD-based models of velocity and nonlinear forcing can be substituted into (6) to yield

$$\sum_{i=1}^{r} \psi_i^u(\boldsymbol{x})\sigma_i^u\phi_i^u(t) = \mathcal{R}\sum_{i=1}^{r} \psi_i^f(\boldsymbol{x})\sigma_i^f\phi_i^f(t), \tag{13}$$

in which the orthonormality in time can be exploited by multiplying both sides by $\phi_i^u(t)$ and averaging in time to obtain

$$\psi_i^u(\boldsymbol{x})\sigma_i^u = \mathcal{R}\sum_{j=1}^{r} \psi_j^f(\boldsymbol{x})\sigma_j^f C_{ij}, \tag{14}$$

where C_{ij} is a matrix representing the correlation between the temporal evolution of the velocity and the nonlinear forcing POD modes. This temporal POD-based filter step can be interpreted as an analogous Fourier transform to obtain (5) from (4). In general, C_{ij} is a dense matrix, however, for the particular case of a periodic flow, C_{ij} would be sparse owing to triadic interactions between dominant and harmonic frequencies. In addition, it is required that for each ith velocity POD mode

$$\sum_{j=1}^{r} C_{ij}^2 \simeq 1, \tag{15}$$

which represents the idea that the rank r is large enough to capture most of the nonlinear forcing driving the fluctuating energy. For ease of explanation in the results that follow, we rewrite (14) with each POD velocity mode as $\boldsymbol{u}_i(\boldsymbol{x}) = \psi_i^u(\boldsymbol{x})\sigma_i^u$ and their corresponding sum of correlated POD forcing modes is substituted as

$$\boldsymbol{f}_i(\boldsymbol{x}) = \sum_{j=1}^{r} \psi_j^f(\boldsymbol{x})\sigma_j^f C_{ij} \tag{16}$$

to yield

$$\boldsymbol{u}_i(\boldsymbol{x}) = \mathcal{R}\boldsymbol{f}_i(\boldsymbol{x}), \tag{17}$$

which represents a discrete-time-domain generalization of the original resolvent formulation [7], as sketched in Fig. 1(b) as an aid to interpretation. In addition, the present framework is linked to the work of Sharma *et al.* [13], where the resolvent operator is interpreted as the linear mapping between velocity and forcing Koopman modes.

The present framework enables the identification of the forcing that excites the most energetic structures in the flow in a time-domain context. The flow structure of $\boldsymbol{f}_i(\boldsymbol{x})$ indicates the spatial location where the nonlinear forcing drives each POD velocity mode $\boldsymbol{u}_i$. A clear passive flow control strategy emerges from this observation: The self-sustained interactions can be interrupted by suppressing the forcing. As such, a passive device could be placed in the spatial location where $\boldsymbol{f}_i(\boldsymbol{x})$ is significant in order to suppress the velocity fluctuations.

We remark that the use of passive device not only inhibits the fluctuations in a specific region, but also modifies the operator $\mathcal{R}$ via changes in the mean flow. This issue is related to the work of Luhar *et al.* [14,15], in which they modeled various active flow control strategies by acting on the boundary conditions of the resolvent operator. The results were in good agreement with previous investigations, despite no corrections being introduced in the mean flow. Consequently, the effect of modifications of the mean flow on $\mathcal{R}$ can be disregarded in a first approximation.

Next we apply this strategy to the periodic flow past a square cylinder. This example represents a good trade-off between complexity of flow structure and computational affordability and it has already been employed in different flow control studies with passive devices [2–5]. A direct numerical simulation of the flow at $\mathrm{Re} = 100$ has been carried out using a spectral-element solver. At this Re, the flow exhibits a Kármán vortex street with a dominant nondimensional frequency

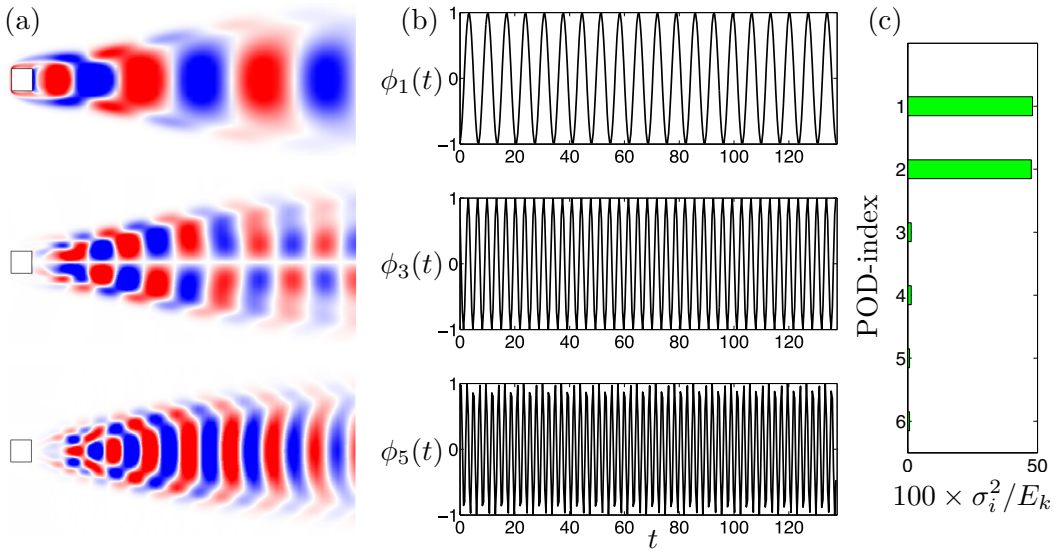

FIG. 2. Fluctuating velocity POD modes. Rows, from top to bottom, show the first, third, and fifth POD mode (a) spatial structure $\psi_i^u(\boldsymbol{x})$, showing vorticity $\omega_z = \pm 0.5$, (b) temporal coefficients $\phi_i^u(t)$, and (c) percentage of kinetic energy corresponding to each POD mode. Note that because of the periodic nature of the flow, POD modes emerge as pairs to account for real and imaginary parts. The mean fluctuating kinetic energy is defined as $E_k = \sum_{i=1}^{s} \sigma_i^2$.

$\mathrm{St} = fD/U = 0.145$. Details of the computation can be found in Ref. [16]; the simulations are converged using the same unstructured mesh consisting of 236 elements with a polynomial degree of 9 and a second-order time integration with a time step $\Delta t = 0.008$. A fixed velocity is imposed at the inlet $\hat{\boldsymbol{u}} = (1,0)$, Neumann boundary conditions are applied at the outlet, and no-slip conditions are imposed at the cylinder surfaces. The computational domain used is $-16 < x < 20$ and $-16 < y < 16$, where $\boldsymbol{x} = (0,0)$ corresponds to the cylinder centroid.

After achieving a periodic state in the simulation, 320 snapshots have been collected equidistributed during 20 vortex shedding periods. The fluctuating component of each snapshot has been computed by subtracting the mean flow and the nonlinear forcing snapshots have been computed using the same spectral-element discretization of the DNS. In a similar manner to the fluctuating velocity, the Reynolds stress $\boldsymbol{f}_0$ must be computed and subtracted from the nonlinear terms $\hat{\boldsymbol{f}}$ in order to get the fluctuating component $\boldsymbol{f}$. A POD of the snapshot matrices has been carried out using a randomized SVD [17]. The results of the POD for the velocity snapshot matrix are summarized in Fig. 2. Because of the periodic nature of the flow, POD modes emerge as pairs to account for real and imaginary parts and these could be merged into a single mode $\boldsymbol{u}_i' = \boldsymbol{u}_i + i\boldsymbol{u}_{i+1}$ using a complex variable. The kinetic energy of each POD mode σ_i^2, represented in Fig. 2(c), indicates that the wake is strongly dominated by the first and second POD modes, which are also associated with the main shedding frequency $\mathrm{St} = 0.145$.

In order to control the wake, we focus on neutralizing the first and second POD modes by identifying the corresponding forcing that excites that modes. Figure 3(a) shows the kinetic energy corresponding to each the forcing POD modes $\boldsymbol{\phi}_i^f(\boldsymbol{x})$ and Fig. 4 shows the correlation matrix of these POD modes with the response POD modes. The correlation matrix C shows that the forcing contribution to the first and second velocity POD modes comes from the third and fourth forcing POD modes; C also highlights how the POD modes emerge as complex conjugate pairs. Note that this particular matrix structure is caused by the periodicity of the flow; as such, this simple structure is not expected in more complex flows. In addition, the correlation satisfies that $\sum_{j=1}^{r} C_{ij}^2 \simeq 1$ for

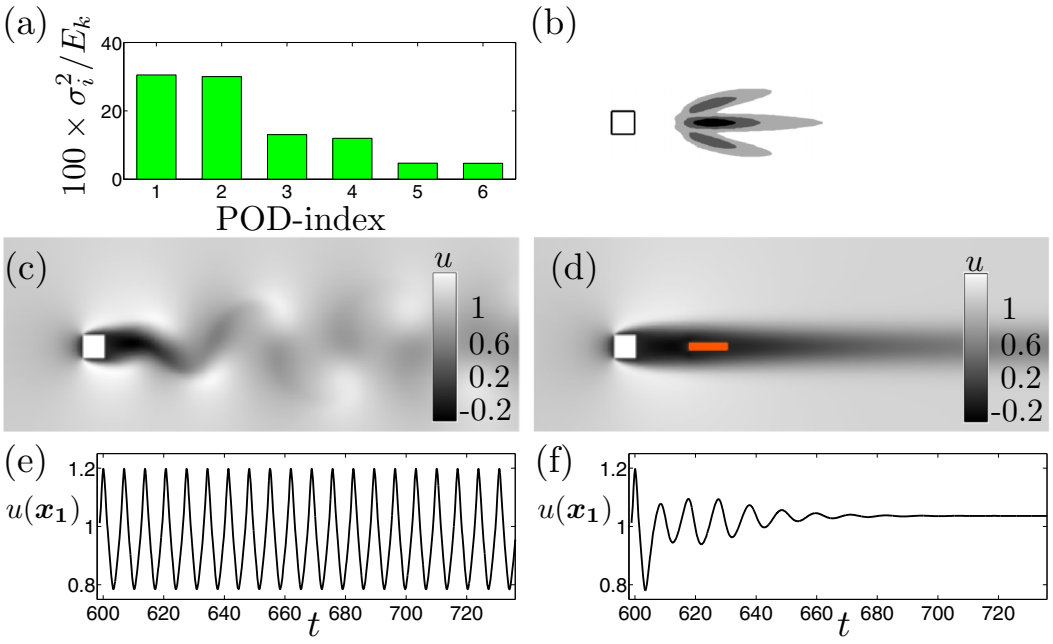

FIG. 3. (a) Percentage of kinetic energy corresponding to each forcing POD mode $\psi_i^f(\boldsymbol{x})$. (b) Contour levels (light gray to black indicate 25%, 50%, and 75%) of the correlated POD forcing mode $|\boldsymbol{f}_1 + i\boldsymbol{f}_2|^2$ driving the oscillatory wake. (c) Snapshot of the uncontrolled flow at $t = 740$, showing streamwise velocity. (d) Snapshot of the controlled flow at $t = 740$, showing streamwise velocity. The passive device is colored in orange. (e) Temporal evolution of the streamwise velocity u at $\boldsymbol{x}_1 = (10, 1.8)$. (f) Temporal evolution of the streamwise velocity u at $\boldsymbol{x}_1 = (10, 1.8)$.

all the considered POD modes, thus the r rank truncation is adequate. This result is consistent with other POD Galerkin models [18], in which the need to consider more than two POD modes to account for higher-order harmonics is highlighted.

Figure 3(d) presents the spatial structure of the correlated POD mode $|\boldsymbol{f}_1 + i\boldsymbol{f}_2|^2$, constructed from (16). This spatial structure consists of three lobes and indicates the locations in which the forcing is produced. We note than the forcing is most concentrated in the central lobe, hence we target that area with a passive device. As a proof of concept, we apply a body force $-m\hat{\boldsymbol{u}}$ in a rectangular subdomain ($3.2 < x < 4.8, -0.15 < y < 0.15$), colored in orange in Fig. 3(c). This body force imposes the velocity to be zero in the application domain, so effectively it acts as a passive device.

$$C \simeq \begin{pmatrix} \epsilon & \epsilon & 0.879 & -0.477 & \epsilon & \epsilon \\ \epsilon & \epsilon & -0.477 & -0.879 & \epsilon & \epsilon \\ 0.677 & -0.736 & \epsilon & \epsilon & \epsilon & \epsilon \\ -0.736 & -0.677 & \epsilon & \epsilon & \epsilon & \epsilon \\ \epsilon & \epsilon & \epsilon & \epsilon & -0.543 & -0.839 \\ \epsilon & \epsilon & \epsilon & \epsilon & -0.839 & 0.543 \end{pmatrix}$$

FIG. 4. Structure of the correlation matrix C. The third and fourth forcing POD modes drive the periodic wake (first and second velocity POD modes). The POD modes emerge as complex conjugates due to the flow periodicity. All columns satisfy that $\sum_{j=1}^{r} C_{ij}^2 \simeq 1$. Here ϵ represent elements of $O(10^{-3})$.

The effect of this device on the flow can be seen in Figs. 3(c)–3(e). In the absence of the device, the flow exhibits periodic vortex shedding. However, if the device is installed in the wake, the flow becomes steady in a few periods. This demonstrates the effectiveness of the proposed flow control strategy.

We note that although the method does not provide the optimal shape and location to inhibit the fluctuation, it provides a useful theoretical background for interpretation of many previous studies. Thus a pleasing connection can be established between the present results and the successful application of splitter plates to control the wake past a square cylinder at similar Reynolds numbers [2–5].

For instance, the spatial structure of the correlated forcing POD mode in Fig. 2(d) justifies why the vortex shedding disappears only when the length of a splitter plate (attached to the cylinder) is larger than $5D$, as shown in Refs. [2,3]. Moreover, the present spatial structure also explains why the attempted control with a splitter plate located between $2.37 < x < 3.2$ by Doolan [4] proved unsuccessful in suppressing unsteadiness; the fluctuating Reynolds stresses driving the wake were generated further downstream.

The spatial structure in Fig. 2(d) is also in qualitative agreement with the study of Zhou *et al.* [5] on suppressing the oscillatory motion of the wake by placing a vertical flat plate upstream of the squared cylinder. Two conditions were required for the success of this flow control strategy: a spacing between the vertical plate and the squared cylinder of at least $3D$ and a height of the vertical flat plate larger than $0.7D$. We hypothesize that in this case the square cylinder acted as a passive device to suppress the fluctuating motion of the wake past the vertical flat plate, consistent with Fig. 2(d).

In conclusion, the results contained in this Rapid Communication demonstrate the success and potential of the proposed approach to design passive flow control strategies. Furthermore, the data-driven nature of the approach makes amenable the use of experimental data and the application of this approach in more complex geometries can proceed similarly. Therefore, the present approach opens up an avenue for the design of flow control using passive devices in a broad range of flows.

The authors acknowledge financial support from the Australian Research Council through Grant No. DP130103103 and from Australia's National Computational Infrastructure via Merit Allocation Scheme Grant No. D77. Stimulating discussions with Prof. Tim Colonius are also acknowledged.

[1] H. Choi, W. P. Jeon, and J. Kim, Control of flow over a bluff body, Annu. Rev. Fluid Mech. **40**, 113 (2008).

[2] K. Kwon and H. Choi, Control of laminar vortex shedding behind a circular cylinder using splitter plates, Phys. Fluids **8**, 479 (1996).

[3] M. S. M. Ali, C. J. Doolan, and V. Wheatley, Low Reynolds number flow over a square cylinder with a splitter plate, Phys. Fluids **23**, 033602 (2011).

[4] C. J. Doolan, Flat-plate interaction with the near wake of a square cylinder, AIAA J. **47**, 475 (2009).

[5] L. Zhou, M. Cheng, and K. C. Hung, Suppression of fluid force on a square cylinder by flow control, J. Fluids Struct. **21**, 151 (2005).

[6] F. Giannetti and P. Luchini, Structural sensitivity of the first instability of the cylinder wake, J. Fluid Mech. **581**, 167 (2007).

[7] B. J. McKeon and A. S. Sharma, A critical layer framework for turbulent pipe flow, J. Fluid Mech. **658**, 336 (2010).

[8] R. Moarref, A. S. Sharma, J. A. Tropp, and B. J. McKeon, Model-based scaling of the streamwise energy density in high-Reynolds-number turbulent channels, J. Fluid Mech. **734**, 275 (2013).

[9] F. Gómez, H. M. Blackburn, M. Rudman, A. S. Sharma, and B. J. McKeon, A reduced-order model of three-dimensional unsteady flow in a cavity based on the resolvent operator, J. Fluid Mech. **798**, R2 (2016).

[10] F. Gómez, A. S. Sharma, and H. M. Blackburn, Estimation of unsteady aerodynamic forces using pointwise velocity data, J. Fluid Mech. **804**, R4 (2016).

[11] S. Beneddine, D. Sipp, A. Arnault, J. Dandois, and L. Lesshafft, Conditions for validity of mean flow stability analysis, J. Fluid Mech. **798**, 485 (2016).

[12] A. Towne, T. Colonius, P. Jordan, A. Cavalieri, and G. A. Brès, in *Proceedings of the 21st AIAA/CEAS Aeroacoustics Conference* (AIAA, Reston, 2015), paper 2015-2217.

[13] A. S. Sharma, I. Mezic, and B. J. McKeon, On the correspondence between Koopman mode decomposition, resolvent mode decomposition, and invariant solutions of the Navier-Stokes equations, Phys. Rev. Fluids **1**, 032402(R) (2016).

[14] M. Luhar, A. S. Sharma, and B. J. McKeon, Opposition control within the resolvent analysis framework, J. Fluid Mech. **749**, 597 (2014).

[15] M. Luhar, A. S. Sharma, and B. J. McKeon, A framework for studying the effect of compliant surfaces on wall turbulence, J. Fluid Mech. **768**, 415 (2015).

[16] H. M. Blackburn and J. M. Lopez, On three-dimensional quasiperiodic Floquet instabilities of two-dimensional bluff body wakes, Phys. Fluids **15**, L57 (2003).

[17] N. Halko, P. G. Martinsson, and J. A. Tropp, Finding structure with randomness: Probabilistic algorithms for constructing approximate matrix decompositions, SIAM Rev. **53**, 217 (2011).

[18] B. R. Noack, K. Afanasiev, M. Morzyński, G. Tadmor, and F. Thiele, A hierarchy of low-dimensional models for the transient and post-transient cylinder wake, J. Fluid Mech. **497**, 335 (2003).